Analytical Model for Phonon Transport Analysis of Periodic Bulk Nanoporous Structures

Qing Hao,* Yue Xiao, Hongbo Zhao

Department of Aerospace and Mechanical Engineering, University of Arizona

Tucson, AZ 85721-0119

Electronic mail: qinghao@email.arizona.edu

(Submitted on March 15, 2016)

Abstract

Phonon transport analysis in nano- and micro-porous materials is critical to their energy-related applications. Assuming diffusive phonon scattering by pore edges, the lattice thermal conductivity can be predicted by modifying the bulk phonon mean free paths with the characteristic length of the nanoporous structure, i.e., the phonon mean free path (Λ_{Pore}) for the pore-edge scattering of phonons. In previous studies (Jean et al., 2014), a Monte Carlo (MC) technique have been employed to extract geometry-determined Λ_{Pore} for nanoporous bulk materials with selected periods and porosities. In other studies (Minnich and Chen, 2007; Machrafi and Lebon, 2015), simple expressions have been proposed to compute Λ_{Pore}. However, some divergence can often be found between lattice thermal conductivities predicted by phonon MC simulations and by analytical models using Λ_{Pore}. In this work, the effective Λ_{Pore} values are extracted by matching the frequency-dependent phonon MC simulations with the analytical model for nanoporous

bulk Si. The obtained Λ_{Pore}values are usually smaller than their analytical expressions. These new values are further confirmed by frequency-dependent phonon MC simulations on nanoporous bulk Ge. By normalizing the volumetric surface area A and Λ_{Pore} with the period length p, the same curve can be used for bulk materials with aligned cubic or spherical pores up to dimensionless $p \cdot A$ of 1.5. Available experimental data for nanoporous Si materials are further analyzed with new Λ_{Pore} values. In practice, the proposed model can be employed for the thermal analysis of various nanoporous materials and thus replace the time-consuming phonon MC simulations.

Keywords: Porous materials, phonon transport, pore-phonon mean free path

Nomenclature

A	Volumetric surface area [1/m]
A^*	Volumetric surface area times period of porous structures [-]
c	Differential volumetric specific heat of phonons [J/K·m^3·(rad/s)]
d	Diameter of spherical pores [m]
F	Porosity-related correction factor of thermal conductivity [-]
k	Thermal conductivity [W/m·K]
N	Number of phonons [-]
p	Period of a periodic porous structure [m]
S	Surface area [m^2]
T	Absolute temperature [K]
t	Time [s]
V	Solid-region volume [m^3]

v_g Phonon group velocity [m/s]

Greek symbols

α Seebeck coefficient [μV/K]

Δ Difference [-]

Λ Phonon mean free path [m]

Λ^* Phonon mean free path times period of porous structure [-]

σ Electrical conductivity [S/m]

τ Phonon relaxation time [s]

φ Volumetric porosity [-]

ω Phonon angular frequency [rad/s]

Subscripts

Bulk Bulk

cyl Cylindrical pores

E Electronic

i Phonon branch

L Lattice

max Maximum

N Normal process

Pore Pore edge

Scatt Scattered

sph Spherical pores

U Umklapp process

Abbreviation

MBL Mean beam length

MC Monte Carlo

MCRT Monte Carlo ray tracing

MD Molecular dynamics

MFP Mean free path

ZT Thermoelectric figure of merit

1. Introduction

In recent years, nano- to micro-porous materials have been widely studied for applications such as thermoelectrics [1-13], photo-luminescence [14], solar cells [15], sensors [16], and thermal management [17, 18]. The large surface-to-volume ratio of nanoporous materials leads to transport properties that are strongly affected by nanopores. In particular, the nanopore scattering of phonons often leads to a dramatically reduced lattice thermal conductivity k_L compared with the bulk value. This may deteriorate the performance of a solar cell due to poor heat spreading and the consequential overheating. In thermoelectrics, however, such k_L reduction is actively pursued to achieve a high thermoelectric figure of merit (ZT), defined as $ZT = \alpha^2\sigma T/k$, where α, σ, k, and T represent Seebeck coefficient, electrical conductivity, thermal conductivity, and absolute temperature, respectively [19]. Here k can be further split into lattice contribution k_L and electronic contribution k_E. Experimentally, it is found that introducing pores in a bulk

material or thin film can largely reduce k_L but still maintain bulk-like power factor $\alpha^2\sigma$, resulting in ZT enhancement [1, 20]. For a Si film with hexagonally packed pores, ZT~0.4 has been achieved at room temperature, in which the measured k values (1.14 to 2.03 W/m·K) are two orders of magnitude lower than that of the bulk Si (150 W/m·K) [1]. Beyond Si, nanoporous materials enable high thermoelectric performance in many other unconventional thermoelectric materials with an intrinsically high k_L.

Numerous studies have been carried out on the phonon transport analysis of micro- to nano-porous bulk materials. For ~10 nm or smaller structures, molecular dynamics (MD) simulations have been conducted for k_L predictions [10, 11, 21-26]. For larger nanoporous structures, phonon Monte Carlo (MC) simulations are employed, in which the exact structure geometry and frequency-dependent phonon mean free paths (MFPs) can both be incorporated [3, 27-29]. Other approaches include the discrete ordinate method [12, 30, 31], hybrid lattice dynamics-continuum mechanics technique [13, 32], and various analytical models [13, 24, 33-36].

Above room temperature, the roughness of pore edges is typically comparable or much larger than the dominant phonon wavelength (~1 nm or less [19]) so that the opportunity for phonons to be specularly reflected by pore edges is very small. In this situation, completely diffusive boundary scattering is assumed in analytical models [24, 31-34] and phonon MC simulations [3, 27-29]. Although this assumption is reasonable for bulk porous materials, challenges are found in explaining the ultra-low k_L observed in periodic nanoporous Si thin films [1, 4-6, 8, 9]. Two major mechanisms are further proposed to explain this divergence. First, periodic nanopores can lead to modified phonon dispersion due to the coherent interference of phonons reflected by pore edges, which will

reduce the phonon group velocities and therefore k_L [5, 8, 13]. In superlattices, this so-called "phononic effect" leads to lower k_L due to phonons reflection by periodic interfaces [37-39]. However, phononic effects are anticipated to be weak in the measured nanoporous films with a period (34 nm to micrometers) that is much larger than the dominant phonon wavelength (~1 nm for Si at 300 K) [6, 18, 27]. This argument is supported by the recent work, in which the measured k_L for nanoporous films with feature sizes larger than 100 nm can be reasonably explained using more reliable frequency-dependent bulk phonon MFPs [29]. Other than phononic effects, the second mechanism for k_L reduction is based on the pore-edge amorphization that will lower k_L by introducing more non-propagating, diffusive lattice-vibration modes [11]. Such amorphization region can usually be introduced by deep reactive ion etching during the pore-drilling process. In addition, an amorphous native oxide layer on pore surfaces [1] can also reduce k_L. In a simple treatment, the effective pore sizes can be expanded with surface amorphization and oxidation on pore edges. Under the assumption of diffusive pore-edge phonon scattering, the experimental data for around 10 nm pore sizes [8] can be reasonably explained by slightly expanded pore sizes [27].

In general, diffusive pore-edge phonon scattering is still a reasonable assumption for phonon transport analysis of porous structure sizes larger than tens of nanometers. Considering classical phonon size effects, nanopores mainly reduce the bulk phonon MFPs with the mean traveling distance of phonons between pore edges, i.e., the phonon MFP Λ_{Pore} corresponding to the pore-edge phonon scattering. This Λ_{Pore} plays a similar role as the nanowire diameter or thin-film thickness in reducing phonon MFPs [40]. For cubically aligned spherical pores, this Λ_{Pore} can be estimated with a simple model [41] but the prediction does not capture the correct trend when the volumetric porosity φ approaches

1 [33]. As a more general approach, Λ_{Pore} has been extracted from the MC ray tracing (MCRT) method that only tracks the pore-edge scattering of phonons within the porous structure [42]. However, only Λ_{Pore} of very limited porous structures have been computed, which does not provide enough guidance for phonon transport analysis of various porous structures. Despite the correct trend of phonon size effects, divergence can often be found between k_L values calculated from analytical models using these Λ_{Pore} values and from phonon MC simulations considering detailed phonon transport within the material [41, 42]. Corrections of Λ_{Pore} values are required to improve the accuracy of k_L predictions. However, this has not been carried out yet.

Without extracting the Λ_{Pore} value, the reduced phonon MFPs or their ratio with the bulk phonon MFPs can also be obtained from MCRT that tracks both phonon-boundary and phonon-phonon scattering events [6, 43]. The latter MFP ratio is called the conductivity reduce function. Within each time step, the shortest traveling distance of phonons by all scattering mechanisms is selected and averaged to yield the reduced phonon MFPs. These MFPs can then be input into the analytical model for k_L predictions, with all other parameters unchanged from the bulk material. When frequency-dependent phonon MFPs are considered, such simulations must be carried out for different bulk phonon MFPs and can be very time-consuming for general thermal analysis of nanoporous materials. Alternatively, the conductivity reduce function of phonon MFPs can also be obtained by numerically integrating the analytical solution for a given bulk phonon MFP and structure geometry [44, 45]. Again this is complicated for three-dimensional geometry and frequency-dependent phonon MFPs.

In this work, Λ_{Pore} for periodic porous bulk structures are extracted by matching k_L predicted by the analytical model and frequency-dependent phonon MC simulations. The obtained Λ_{Pore} is generally lower than previous predictions, particularly at low porosities. For different porosity φ and period p, the same curve can be used to describe the relationship between dimensionless $\Lambda_{Pore}^{*} = \Lambda_{Pore}/p$ and volumetric surface area $A^{*}=pA$ for bulk materials with cubic or spherical pores, except for small divergence at $A^{*}>1.5$. **The usage of Λ_{Pore}^{*} leads to a unified picture of porous bulk materials with different structure periods, whereas previous studies only deal with limited porous structure dimensions and thus lose the generality [42].** The developed model agrees well with frequency-dependent phonon MC simulations and is further applied to the data analysis of measured nanoporous Si materials of various structure sizes. Instead of time-consuming phonon MC simulations, this simple model can be widely used for the phonon transport analysis of various nano- to micro-porous structures.

2. Theory/calculation

2.1 Analytical model for k_L calculations

The lattice thermal conductivity k_L of a nanoporous material is computed based on the kinetic relationship [19],

$$k_L = \frac{F(\varphi)}{3}\sum_{i=1}^{3}\int_0^{\omega_{max,i}} c_i(\omega)v_{g,i}(\omega)\Lambda_i(\omega)d\omega, \quad (1)$$

where the subscript i indicates the phonon branch, φ is the porosity, ω is the phonon angular frequency, $c_i(\omega)$ is the differential volumetric phonon specific heat, $v_{g,i}(\omega)$ is the phonon group velocity for branch i and angular frequency ω, $F(\varphi)$ is the correction factor for porosity φ, and $\Lambda_i(\omega)$ is the effective phonon MFP. Only three acoustic branches are

considered here because the optical phonon contribution is negligible due to their small group velocities. For cubically aligned spherical pores, the factor $F(\varphi)$ is given by Eucken as

$$F(\varphi)=(1-\varphi)/(1+\varphi/2), \quad (2)$$

to account for the porosity influence [46, 47]. When cubic pores are considered, the Russell factor [48] should be used, given as

$$F(\varphi)=(1-\varphi^{2/3})/(1+\varphi-\varphi^{2/3}). \quad (3)$$

Assuming diffusive phonon scattering by pore edges, $\Lambda_i(\omega)$ is modified from the bulk value $\Lambda_{Bulk,i}(\omega)$ based on the Matthiessen's rule:

$$1/\Lambda_i(\omega) = 1/\Lambda_{Bulk,i}(\omega) + 1/\Lambda_{Pore}\ , \quad (4)$$

in which Λ_{Pore} is the phonon MFP due to diffusive pore edge scattering of phonons. For a given nanoporous structure, lattice thermal conductivity can be easily predicted when Λ_{Pore} is determined.

2.2 Available expressions of Λ_{Pore}

For k_L computations, analytical models for Λ_{Pore} have been derived in previous studies. Considering spherical nanoinclusions embedded in a bulk material, Λ_{Pore} is given as [41]

$$\Lambda_{Pore,sph} = \frac{4p^3}{d^2} = \frac{2d}{3\varphi}, \quad (5)$$

Where the subscript "sph" indicates spherical pores, p is the period of the structure, and d is the diameter of nanopores or nanoparticle inclusions. Equation (5) becomes invalid when φ is close to 1. In this case, phonons mainly flow along the channel between adjacent pores and Λ_{Pore} approaches zero for very narrow channel width. In contrast, Eq. (5)

predicts nonzero Λ_{Pore}=2d/3 for $\varphi \approx 1$. To address this conflict for the $\varphi \to 1$ limit, an additional factor is multiplied to Λ_{Pore} [33] so that Eq. (5) becomes

$$\Lambda_{Pore,sph} = \frac{2(1-\varphi)d}{3\varphi}. \quad (6)$$

In radiation, Λ_{Pore} can also be estimated by the optically thin limit of the mean beam length (MBL) for an enclosure, given as [49]

$$\Lambda_{Pore,sph} = \frac{4V}{S} = \frac{4}{A}(1-\varphi)\,, \quad (7)$$

where the solid-region volume V and surface area S can be evaluated for a given porous structure. The ratio between S and V is further related to the volumetric surface area A. It can be shown that Eq. (6) is equivalent to Eq. (7) for a bulk material with periodic spherical pores. However, Eq. (7) can be more general and can be applied to porous materials with arbitrary pore shapes.

2.3 Extracting Λ_{Pore} from MCRT

In principle, Λ_{Pore} only depends on the geometry of the porous structure and is unchanged for different phonon frequencies and branches [42]. This value can be extracted from MCRT by tracking a large number N of phonons randomly moving within a single period of the porous structure that is used as the computational domain. In these simulations, only pore-edge phonon scattering is considered and all phonons have ballistic transport before hitting pore edges or the domain boundary. As shown in Fig. 1, phonons incident on pore edges will be randomized for their traveling directions after diffusive pore-edge scattering, with all other parameters unchanged [3, 50]. This random resetting of phonon traveling directions has been discussed for cubic pores [3, 50]. For spherical pores, the detail of the direction resetting is given in the Appendix. To be consistent with phonon

MC simulations for k_L predictions, phonons incident on the sidewall of the domain boundary will be specularly reflected. Phonons hitting the left or right boundaries of the domain will re-enter the domain from the opposite boundary by shifting the x coordinate, with the same phonon group velocity and traveling direction.

To simplify, the same phonon group velocity v_g is assigned to all phonons. Within a time step Δt, the number of phonons diffusively scattered by pore edges (N_{scatt}) will be recorded so that Λ_{Pore} can be computed by [51]

$$\Lambda_{Pore} = \frac{v_g \Delta t}{ln(\frac{N}{N-N_{scatt}})}. \quad (8)$$

In the proposed simulations, several million phonons are randomly distributed in the computational domain. The simulations are carried out for more than 10,000 time steps and the obtained Λ_{Pore} is averaged to improve the accuracy. For representative cases, the phonon number in simulations is also increased to ~80 million and Λ_{Pore} is also computed after running the simulations for 10 nanoseconds. The obtained Λ_{Pore} values typically change within 1‰, which confirms the precision of Λ_{Pore}.

Notably, an extremely good agreement can be found between the MBL values of Eq. (7) and the Λ_{Pore} values extracted by MCRT, regardless the shape of nanopores (Fig. 2). In principle, the MCRT-extracted Λ_{Pore} is the pore-edge-scattering MFPs of phonons starting from any points within a porous structure, while the MBL is the characteristic length for phonon radiation between pore edges. Despite such difference, in practice the MBL Λ_{Pore} can be used to replace MCRT Λ_{Pore} that requires complicated simulations.

2.4 Extracting Λ_{Pore} by comparing phonon MC simulations with the analytical model

Along another line, Λ_{Pore} can be extracted by directly comparing k_L predicted by the kinetic relation in Eq. (1) and frequency-dependent phonon MC simulations. By tracking the heat flow across the computational domain with applied temperature difference, k_L of arbitrary structures can be predicted by these phonon MC simulations. In comparison to the MCRT method, this approach is directly related to the analytical model and the extracted effective Λ_{Pore} can be more accurate.

In phonon MC simulations, an isotropic phonon dispersion is assumed and takes the phonon dispersion along the (001) direction for bulk materials such as Si and Ge. As another input parameter, the phonon relaxation time $\tau_i(\omega)$ for branch *i*, defined as $\Lambda_{Bulk,i}(\omega)/v_{g,i}(\omega)$, is computed based on the Matthiessen's rule: ${\tau_i}^{-1}(\omega) = {\tau_I}^{-1}(\omega) + {\tau_{i,N}}^{-1}(\omega) + {\tau_{i,U}}^{-1}(\omega)$, where $\tau_I(\omega)$, $\tau_{i,N}(\omega)$, $\tau_{i,U}(\omega)$ are the relaxation times of impurity scattering, normal (N) process, and Umklapp (U) process, respectively. Here $\tau_{i,N}(\omega)$ and $\tau_{i,U}(\omega)$ are modified from those given by first-principles studies for bulk Si and Ge using the real phonon dispersion in the whole *k* space [52, 53]. **Because the proposed phonon MC simulations assume isotropic phonon dispersion, it is found that the frequency-dependent scattering rates for the N and U processes of transverse acoustic phonons should be both divided by 1.72 to fit the first-principles data for both bulk Si and Ge, with all other parameters unchanged.** The exact expressions and parameters used for bulk Si can also be found in our previous work [54].

3. Results and discussions

This section is organized into three parts. First, ${\Lambda_{Pore}}^*$ is extracted by matching the analytical model in Eq. (1) and frequency-depend phonon MC simulations on nanoporous

bulk Si. Second, the extracted Λ_{Pore}^{*} is compared with available theoretical expressions. Third, the predicted k_L using these Λ_{Pore}^{*} values is compared to reported experimental results.

3.1 Λ_{Pore}^{*} extracted for nanoporous bulk Si and its validation

As a more accurate method, the effective Λ_{Pore}^{*} is directly extracted by matching the prediction of the analytical model in Eq. (1) and frequency-dependent phonon MC simulations. The recently proposed deviational phonon MC simulation technique [55] is used to dramatically improve the computation efficiency. The detail of such simulations can be found in the literature and will not be discussed here. As representative cases, nanoporous bulk Si with cubically aligned cubic or spherical pores is computed. The investigation includes numerous combinations between the porosity φ and period p. For the same φ and pore shape, the dimensionless $\Lambda_{Pore}^{*} = \Lambda_{Pore}/p$ mostly varies within 5% for p from 50 to 500 nm. Figures 3a and 3b present the Λ_{Pore}^{*} curve for bulk Si with cubic and spherical pores. Based on the results, it is anticipated that the normalized Λ_{Pore}^{*} value is only determined by the porosity and is independent of p. Thus an averaged Λ_{Pore}^{*} over various p values is extracted and used in Eq. (4).

The averaged Λ_{Pore}^{*} is further validated with frequency-dependent phonon MC simulations. In Figs. 4a and 4b, the predictions using Λ_{Pore}^{*} (solid lines) for Si with cubic and spherical pores agree well with frequency-dependent phonon MC simulations (symbols). The overall divergence is less than 5%. In Fig. 4c, similar agreement is found for bulk Ge with cubic pores. **It should be noted that Λ_{Pore}^{*} extraction largely depends on the phonon MFP spectrum of bulk materials. For both bulk Si and Ge, their**

frequency-dependent phonon MFPs span from nanometers to millimeters. Similar phonon MFP spectra can also be found in many other materials [56, 57], in which the extracted Λ_{Pore}^{*} is anticipated to be accurate. In contrast, predictions using Λ_{Pore} from the MBL in Eq. (7) or MCRT method leads to larger divergence at porosity of 10–30% for bulk Si and Ge with cubic pores. For spherical pores, the MBL/MCRT predictions are generally higher than those from frequency-dependent phonon MC simulations. **However, Λ_{Pore} by MBL or the MCRT method can still be accurate when extremely strong ballistic phonon transport exists, i.e., bulk materials with ultrafine porous structures and long bulk phonon MFPs.**

3.2 Comparison with other Λ_{Pore}^{*} models

In Fig. 5a, the averaged Λ_{Pore}^{*} for cubic and spherical pores (solid lines) are plotted as a function of the dimensionless A^{*}, which is the product of the volumetric surface area A and the period length p. This dimensionless A^{*}, determined by the porosity φ, is more fundamental for the description of phonon boundary scattering within nanostructures. Except for some divergence at high A^{*} values, the two solid curves for cubic and spherical pores are very close for A^{*}<1.5. This A^{*} range corresponds to φ up to 12.5% and 17.3% for bulk materials with cubic pores and spherical pores, respectively. In comparison, Λ_{Pore}^{*} is also plotted as a function of porosity φ in Fig. 5b and more divergence is found at low porosities. In Figs. 5a and 5b, Λ_{Pore}^{*} calculated by the MBL/MCRT method and Eq. (5) used by Minnich and Chen [41] are also displayed. In general, these expressions predict higher Λ_{Pore}^{*} values. Particularly for Eq. (5), its divergence from other predictions increases at larger A^{*} or φ values, which will lead to much higher k_L values.

The MBL in Eq. (7) can be applied to bulk materials with irregular pores. The exact pore shapes do not affect $\Lambda_{Pore}{}^{*}$ in this case. Similar weak pore-shape dependence of $\Lambda_{Pore}{}^{*}$ is also observed between the two averaged $\Lambda_{Pore}{}^{*}$ curves in Fig. 5a. This trend is found in previous phonon MC simulations of disordered nanograined bulk materials, in which the volumetric grain-boundary area is determined as the major factor for k_L reduction and overshadows the influence of the exact shape and alignment of nanograins [58]. Based on this, computations of bulk materials with arbitrary pore shapes may use similar $\Lambda_{Pore}{}^{*}$ values for the same A^{*}. For two-dimensional nanoporous thin films, more detailed comparison between k_L for different pore shapes and pore alignment can be found in a recent study [59].

3.3 Phonon transport analysis of available experimental data on nanoporous Si

The $\Lambda_{Pore}{}^{*}$ values extracted in Section 3.1 is further used for k_L predictions of nanoporous bulk Si to be compared with the experimental data [60, 61] (Table 1). The $\Lambda_{Pore}{}^{*}$ value for a bulk materials with cubic pores is adopted. The analyzed samples are synthesized by etching bulk Si, resulting in connected irregular pores. Due to the poor electron conduction in these porous samples, electronic contribution k_E can be neglected so that k is close to k_L. The k (k_L) values are measured using a conventional photoacoustic gas-microphone technique [60] or the widely used 3ω technique [61], both of which provide an effective k value averaged over all directions. The same samples have also been analyzed in the previous phonon modeling work on nanoporous bulk materials [33].

The experimental results are compared to the model predictions that are plotted as a function of A^{*} and the averaged pore diameter d (Fig. 6). Despite the difference in pore shapes, little divergence is anticipated for k_L predictions when A^{*} and φ can be matched.

In general, the predicted k values agree reasonably well with these experimental data, except for a sample with pore sizes of 200 nm (diamond dot). It is also found that the predicted k values match better with experimental data at higher φ in Table 1.

4. Conclusions

In this work, dimensionless pore-phonon-scattering MFP ($\Lambda_{Pore}{}^{*}$) is extracted for general nanoporous bulk materials by matching k_L predicted by the kinetic relationship and frequency-dependent phonon MC simulations. For the same pore shape, a single $\Lambda_{Pore}{}^{*} - A^{*}$ curve is identified for different materials and structure sizes.

Using the extracted $\Lambda_{Pore}{}^{*}$, the predicted k_L is in good agreement with the frequency-dependent phonon MC simulations for both nanoporous bulk Si and Ge. The predictions also match existing experimental results. In contrast, $\Lambda_{Pore}{}^{*}$ given by Eqs. (5) –(7) often leads to overestimated k_L, especially at high porosities. It should also be pointed out that the Λ_{Pore} acquired by the MCRT method is practically interchangeable with the MBL for the same structure geometry, despite the difference in their definitions.

With these accurate $\Lambda_{Pore}{}^{*}$ values, the often complicated and time-consuming phonon MC simulations can be replaced by the simple analytical model for both data analysis and materials design. This will greatly facilitate the research for thermoelectrics and other relevant fields, where introducing nanoporosity is widely used as an effective way to reduce k_L.

Acknowledgements

The authors thank Dr. Jean-Philippe M Péraud for the help of deviational phonon MC simulations. An allocation of computer time from the UA Research Computing High

Performance Computing (HTC) and High Throughput Computing (HTC) at the University of Arizona is gratefully acknowledged.

[1] J. Tang, H.-T. Wang, D.H. Lee, M. Fardy, Z. Huo, T.P. Russell, P. Yang, Holey Silicon as an Efficient Thermoelectric Material, Nano Letters, 10 (2010) 4279-4283.
[2] J. Lee, J. Lim, P. Yang, Ballistic Phonon Transport in Holey Silicon, Nano Letters, 15 (2015) 3273-3279.
[3] Q. Hao, G. Chen, M.-S. Jeng, Frequency-dependent Monte Carlo simulations of phonon transport in two-dimensional porous silicon with aligned pores, Journal of Applied Physics, 106 (2009) 114321.
[4] Q. Hao, D. Xu, H. Zhao, Systematic Studies of Periodically Nanoporous Si Films for Thermoelectric Applications, in: P. Hopkins (ed.) 2015 MRS Spring Meeting & Exhibit, Vol. 1779, San Francisco, California, 2015, pp. mrss15-2137995.
[5] P.E. Hopkins, C.M. Reinke, M.F. Su, R.H. Olsson, E.A. Shaner, Z.C. Leseman, J.R. Serrano, L.M. Phinney, I. El-Kady, Reduction in the Thermal Conductivity of Single Crystalline Silicon by Phononic Crystal Patterning, Nano Letters, 11 (2010) 107-112.
[6] A.M. Marconnet, T. Kodama, M. Asheghi, K.E. Goodson, Phonon Conduction in Periodically Porous Silicon Nanobridges, Nanoscale and Microscale Thermophysical Engineering, 16 (2012) 199-219.
[7] B. Kim, J. Nguyen, P.J. Clews, C.M. Reinke, D. Goettler, Z.C. Leseman, I. El-Kady, R. Olsson, Thermal conductivity manipulation in single crystal silicon via lithographycally defined phononic crystals, in: Micro Electro Mechanical Systems (MEMS), 2012 IEEE 25th International Conference on, IEEE, 2012, pp. 176-179.
[8] J.-K. Yu, S. Mitrovic, D. Tham, J. Varghese, J.R. Heath, Reduction of Thermal Conductivity in Phononic Nanomesh Structures, Nature Nanotechnology, 5 (2010) 718-721.
[9] D. Song, G. Chen, Thermal conductivity of periodic microporous silicon films, Applied Physics Letters, 84 (2004) 687-689.
[10] J.H. Lee, J.C. Grossman, J. Reed, G. Galli, Lattice thermal conductivity of nanoporous Si: Molecular dynamics study, Applied Physics Letters, 91 (2007) 223110-223113.
[11] Y. He, D. Donadio, J.-H. Lee, J.C. Grossman, G. Galli, Thermal Transport in Nanoporous Silicon: Interplay between Disorder at Mesoscopic and Atomic Scales, ACS Nano, 5 (2011) 1839-1844.
[12] G. Romano, A. Di Carlo, J.C. Grossman, Mesoscale modeling of phononic thermal conductivity of porous Si: interplay between porosity, morphology and surface roughness, Journal of Computational Electronics, 11 (2012) 8-13.
[13] E. Dechaumphai, R. Chen, Thermal Transport in Phononic Crystals: The Role of Zone Folding Effect, Journal of Applied Physics, 111 (2012) 073508-073508.
[14] A. Cullis, L. Canham, P. Calcott, The structural and luminescence properties of porous silicon, Journal of Applied Physics, 82 (1997) 909-965.
[15] Y. Chao, Optical properties of nanostructured silicon, Comprehensive Nanoscience and Technology, (2011) 543.

[16] P. Granitzer, K. Rumpf, Porous silicon—a versatile host material, Materials, 3 (2010) 943-998.
[17] T.W. Clyne, I.O. Golosnoy, J.C. Tan, A.E. Markaki, Porous materials for thermal management under extreme conditions, Philosophical Transactions of the Royal Society of London A: Mathematical, Physical and Engineering Sciences, 364 (2006) 125-146.
[18] M. Maldovan, Narrow Low-Frequency Spectrum and Heat Management by Thermocrystals, Physical Review Letters, 110 (2013) 025902.
[19] G. Chen, Nanoscale Energy Transport and Conversion: A Parallel Treatment of Electrons, Molecules, Phonons, and Photons, Oxford University Press, New York, 2005.
[20] Q. He, S. Hu, X. Tang, Y. Lan, J. Yang, X. Wang, Z. Ren, Q. Hao, G. Chen, The great improvement effect of pores on ZT in $Co_{1-x}Ni_xSb_3$ system, Applied Physics Letters, 93 (2008) 042108.
[21] L. Yang, N. Yang, B. Li, Extreme low thermal conductivity in nanoscale 3D Si phononic crystal with spherical pores, Nano Letters, 14 (2014) 1734-1738.
[22] J. Fang, L. Pilon, Scaling laws for thermal conductivity of crystalline nanoporous silicon based on molecular dynamics simulations, Journal of Applied Physics, 110 (2011) 064305.
[23] D. Şopu, J. Kotakoski, K. Albe, Finite-size effects in the phonon density of states of nanostructured germanium: A comparative study of nanoparticles, nanocrystals, nanoglasses, and bulk phases, Physical Review B, 83 (2011) 245416.
[24] R. Dettori, C. Melis, X. Cartoixà, R. Rurali, L. Colombo, Model for thermal conductivity in nanoporous silicon from atomistic simulations, Physical Review B, 91 (2015) 054305.
[25] L. Yang, J. Chen, N. Yang, B. Li, Significant reduction of graphene thermal conductivity by phononic crystal structure, International Journal of Heat and Mass Transfer, 91 (2015) 428-432.
[26] J. Chen, G. Zhang, B. Li, A universal gauge for thermal conductivity of silicon nanowires with different cross sectional geometries, The Journal of chemical physics, 135 (2011) 204705.
[27] N.K. Ravichandran, A.J. Minnich, Coherent and incoherent thermal transport in nanomeshes, Physical Review B, 89 (2014) 205432.
[28] J. Randrianalisoa, D. Baillis, Monte Carlo simulation of cross-plane thermal conductivity of nanostructured porous silicon films, Journal of Applied Physics, 103 (2008) 053502.
[29] A. Jain, Y.-J. Yu, A.J.H. McGaughey, Phonon transport in periodic silicon nanoporous films with feature sizes greater than 100 nm, Physical Review B, 87 (2013) 195301.
[30] J.D. Chung, M. Kaviany, Effects of phonon pore scattering and pore randomness on effective conductivity of porous silicon, International Journal of Heat and Mass Transfer, 43 (2000) 521-538.
[31] T.-Y. Hsieh, H. Lin, T.-J. Hsieh, J.-C. Huang, Thermal conductivity modeling of periodic porous silicon with aligned cylindrical pores, Journal of Applied Physics, 111 (2012) 124329.
[32] C.M. Reinke, M.F. Su, B.L. Davis, B. Kim, M.I. Hussein, Z.C. Leseman, R.H. Olsson-III, I. El-Kady, Thermal conductivity prediction of nanoscale phononic crystal slabs using a hybrid lattice dynamics-continuum mechanics technique, AIP Advances, 1 (2011) 041403.

[33] H. Machrafi, G. Lebon, Size and porosity effects on thermal conductivity of nanoporous material with an extension to nanoporous particles embedded in a host matrix, Physics Letters A, 379 (2015) 968-973.
[34] R.H. Tarkhanyan, D.G. Niarchos, Reduction in lattice thermal conductivity of porous materials due to inhomogeneous porosity, International Journal of Thermal Sciences, 67 (2013) 107-112.
[35] R. Prasher, Thermal conductivity of composites of aligned nanoscale and microscale wires and pores, Journal of Applied Physics, 100 (2006) 034307.
[36] R. Prasher, Transverse thermal conductivity of porous materials made from aligned nano-and microcylindrical pores, Journal of Applied Physics, 100 (2006) 064302.
[37] P. Hyldgaard, G. Mahan, Phonon superlattice transport, Physical Review B, 56 (1997) 10754.
[38] M. Simkin, G. Mahan, Minimum thermal conductivity of superlattices, Physical Review Letters, 84 (2000) 927.
[39] S.-i. Tamura, Y. Tanaka, H.J. Maris, Phonon group velocity and thermal conduction in superlattices, Physical Review B, 60 (1999) 2627-2630.
[40] H. Casimir, Note on the Conduction of Heat in Crystals, Physica, 5 (1938) 495-500.
[41] A. Minnich, G. Chen, Modified effective medium formulation for the thermal conductivity of nanocomposites, Applied Physics Letters, 91 (2007) 073105-073103.
[42] V. Jean, S. Fumeron, K. Termentzidis, S. Tutashkonko, D. Lacroix, Monte Carlo simulations of phonon transport in nanoporous silicon and germanium, Journal of Applied Physics, 115 (2014) 024304.
[43] A.J.H. McGaughey, A. Jain, Nanostructure thermal conductivity prediction by Monte Carlo sampling of phonon free paths, Applied Physics Letters, 100 (2012) 061911.
[44] E.H. Sondheimer, The mean free path of electrons in metals, Advances in physics, 50 (2001) 499-537.
[45] R. Chambers, The conductivity of thin wires in a magnetic field, in: Proceedings of the Royal Society of London A: Mathematical, Physical and Engineering Sciences, Vol. 202, The Royal Society, 1950, pp. 378-394.
[46] A. Eucken, Thermal conductivity of ceramic refractory materials: calculation from thermal conductivity of constituents, Ceramic Abstracts, 11 (1932) 576.
[47] A. Eucken, Thermal conductivity of ceramic refractory materials: calculation from thermal conductivity of constituents, Ceramic Abstracts, 12 (1933) 231.
[48] H. Russell, Principles of heat flow in porous insulators*, Journal of the American Ceramic Society, 18 (1935) 1-5.
[49] J.R. Howell, M.P. Menguc, R. Siegel, Thermal radiation heat transfer, CRC press, 2010.
[50] Q. Hao, G. Chen, Frequency-Dependent Monte Carlo Simulations of Phonon Transport in Nanostructures, in: S. Mordechai (ed.) Applications of Monte Carlo Method in Science and Engineering, InTech, 2011.
[51] D. Lacroix, K. Joulain, D. Lemonnier, Monte Carlo transient phonon transport in silicon and germanium at nanoscales, Physical Review B, 72 (2005) 064305.
[52] A. Ward, First principles theory of the lattice thermal conductivity of semiconductors, in: Physics, Vol. Ph.D., Boston College, Boston, 2009.
[53] A. Ward, D.A. Broido, Intrinsic phonon relaxation times from first-principles studies of the thermal conductivities of Si and Ge, Physical Review B, 81 (2010) 085205.

[54] Q. Hao, General effective medium formulation for thermal analysis of a polycrystal—The influence of partially specular phonon transmission across grain boundaries, Journal of Applied Physics, 116 (2014) 034305.
[55] J.-P.M. Péraud, N.G. Hadjiconstantinou, Efficient simulation of multidimensional phonon transport using energy-based variance-reduced Monte Carlo formulations, Physical Review B, 84 (2011) 205331.
[56] J.P. Freedman, J.H. Leach, E.A. Preble, Z. Sitar, R.F. Davis, J.A. Malen, Universal phonon mean free path spectra in crystalline semiconductors at high temperature, Scientific reports, 3 (2013) 2963.
[57] T. Feng, X. Ruan, Prediction of spectral phonon mean free path and thermal conductivity with applications to thermoelectrics and thermal management: a review, Journal of Nanomaterials, 2014 (2014).
[58] Q. Hao, Influence of Structure Disorder on the Lattice Thermal Conductivity of Polycrystals: A Frequency-Dependent Phonon-Transport Study, Journal of Applied Physics, 111 (2012) 014309.
[59] G. Romano, J.C. Grossman, Toward phonon-boundary engineering in nanoporous materials, Applied Physics Letters, 105 (2014) 033116.
[60] G. Benedetto, L. Boarino, R. Spagnolo, Evaluation of thermal conductivity of porous silicon layers by a photoacoustic method, Applied Physics A, 64 (1997) 155-159.
[61] G. Gesele, J. Linsmeier, V. Drach, J. Fricke, R. Arens-Fischer, Temperature-dependent thermal conductivity of porous silicon, Journal of Physics D: Applied Physics, 30 (1997) 2911.

Appendix: Treatment of Spherical Pores in Phonon MC Simulations with Rectangular Subcells

One problem of dealing with spherical pores is that the computational domain is usually divided into rectangular subcells as spatial bins of phonons. The rectangular subcells must be modified to accommodate spherical pores. For subcells intercepting with the pore edge, only the subcell volume outside the pore should be used in the simulation. This partial volume can also be evaluated by the MC technique before the simulation starts. A large number of particles will be randomly distributed within these subcells and the percentage of particles outside the sphere is counted, which equals the percentage of the subcell volume outside the sphere (Fig. A1).

For diffusive phonon reflection by pore edges, the traveling direction of a phonon will be randomly reset. Considering the diffuse reflection by Point A in Fig. A2, the unit vector $\vec{k}_0$ for the new traveling direction is given by

$$\vec{k}_0 = \begin{bmatrix} \sqrt{R_1} \\ \left(\sqrt{1-R_1}\right)\cos(2\pi R_2) \\ \left(\sqrt{1-R_1}\right)\sin(2\pi R_2) \end{bmatrix}, \tag{A1}$$

where R_1 and R_2 are two random numbers between 0 to 1. For phonon reflected at general Point C on the pore edge, the outbound $\vec{k}_f$ can be obtained by rotating $\vec{k}_0$ with angle ϕ in the x-y plane to Point B, and then by angle θ in the x-z plane to Point C. The resulting $\vec{k}_f$ is determined by

$$\vec{k}_f = Y_\theta Z_\Phi \vec{k}_0, \tag{A2}$$

in which

$$Z_{\phi} = \begin{bmatrix} cos\phi & -sin\phi & 0 \\ sin\phi & cos\phi & 0 \\ 0 & 0 & 1 \end{bmatrix},$$

$$Y_{\theta} = \begin{bmatrix} cos\theta & 0 & -sin\theta \\ 0 & 1 & 0 \\ sin\theta & 0 & cos\theta \end{bmatrix}. \quad \text{(A3)}$$

FIGURES AND TABLE

Figure Captions

Figure 1. The middle x-y plane of the simulation domain with spherical pores. The domain is selected as one period of the structure. Phonons hitting the pore edge will be diffusively scattered. Phonons incident on the four sidewalls will be specularly reflected. Phonons incident on the left or right boundaries are shifted to the opposite boundary to continue their movement.

Figure 2. $\Lambda_{Pore}{}^{*}$ obtained with the MCRT method and MBL/*p*, both as functions of porosity.

Figure 3. Porosity- and period-dependent $\Lambda_{Pore}{}^{*}$ as extracted by matching the analytical model in Eq. (1) with frequency-dependent phonon MC simulations on nanoporous bulk Si: a) cubic pores, b) spherical pores.

Figure 4. Lattice thermal conductivities predicted by Eq. (1) using the extracted $\Lambda_{Pore}{}^{*}$ and by frequency-dependent phonon MC simulations: (a) bulk Si with aligned cubic pores, (b) bulk Si with aligned spherical pores, and (c) bulk Ge with aligned cubic pores.

Figure 5. a) Dimensionless $\Lambda_{Pore}{}^{*}$ as a function of: a) the volumetric surface area A^{*} as the product of the volumetric area and the period *p*; and b) the porosity φ. Results of this work are also compared with other predictions.

Figure 6. Comparison between predicted and measured thermal conductivities of nanoporous bulk Si, including results from Refs. [56] (♦ and ▼) and [57] (▲ and ●).

Figure A1. Determination of the out-pore volume for subcells intercepting with the pore edge.

Figure A2. Rotating the outbound direction vector $\vec{k}_0$ from Point A to general Point C. Points A and B are in the x-y plane with z=0. Points B and C are in the same x-z plane.

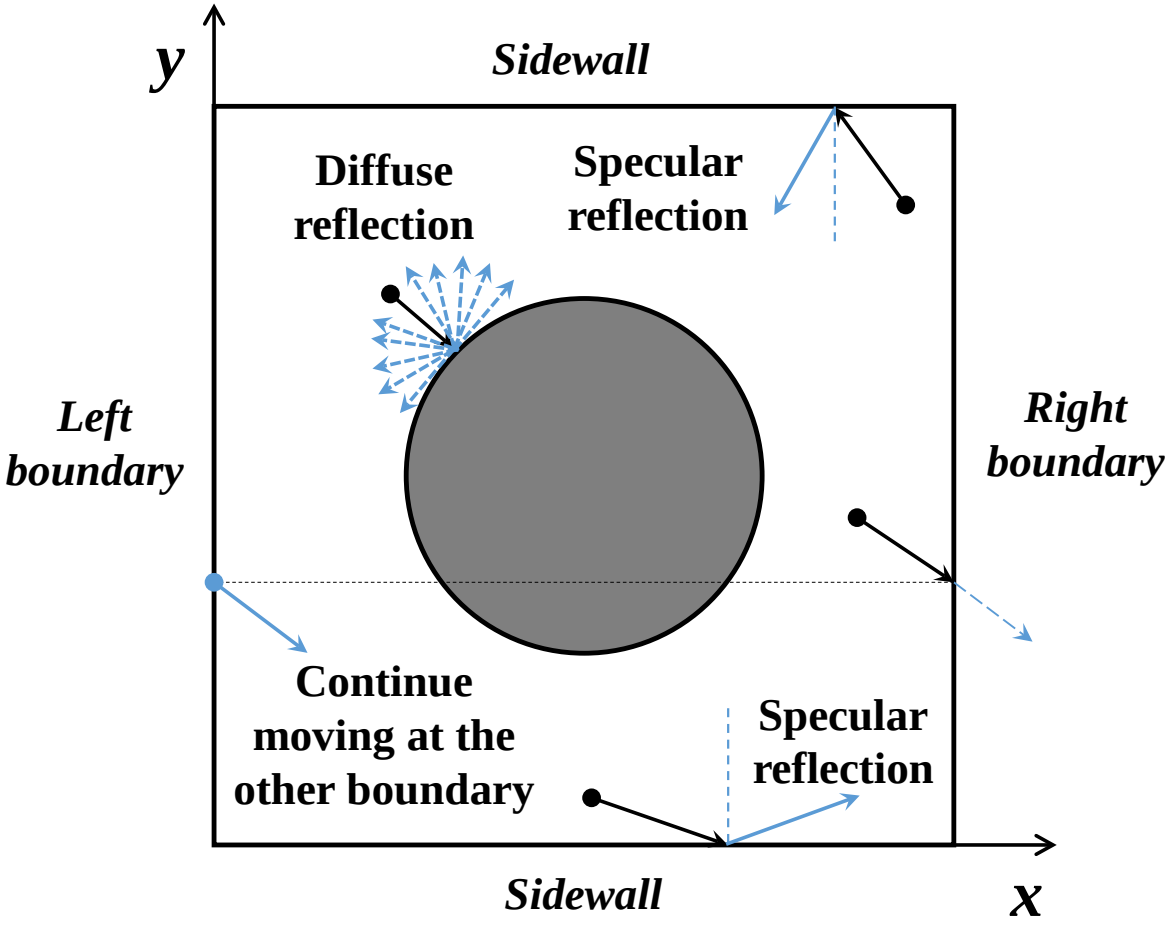
y
Sidewall
Diffuse
reflection
Specular
reflection
Left
boundary
Right
boundary
Continue
moving at the
other boundary
Specular
reflection
Sidewall
x

Figure 1

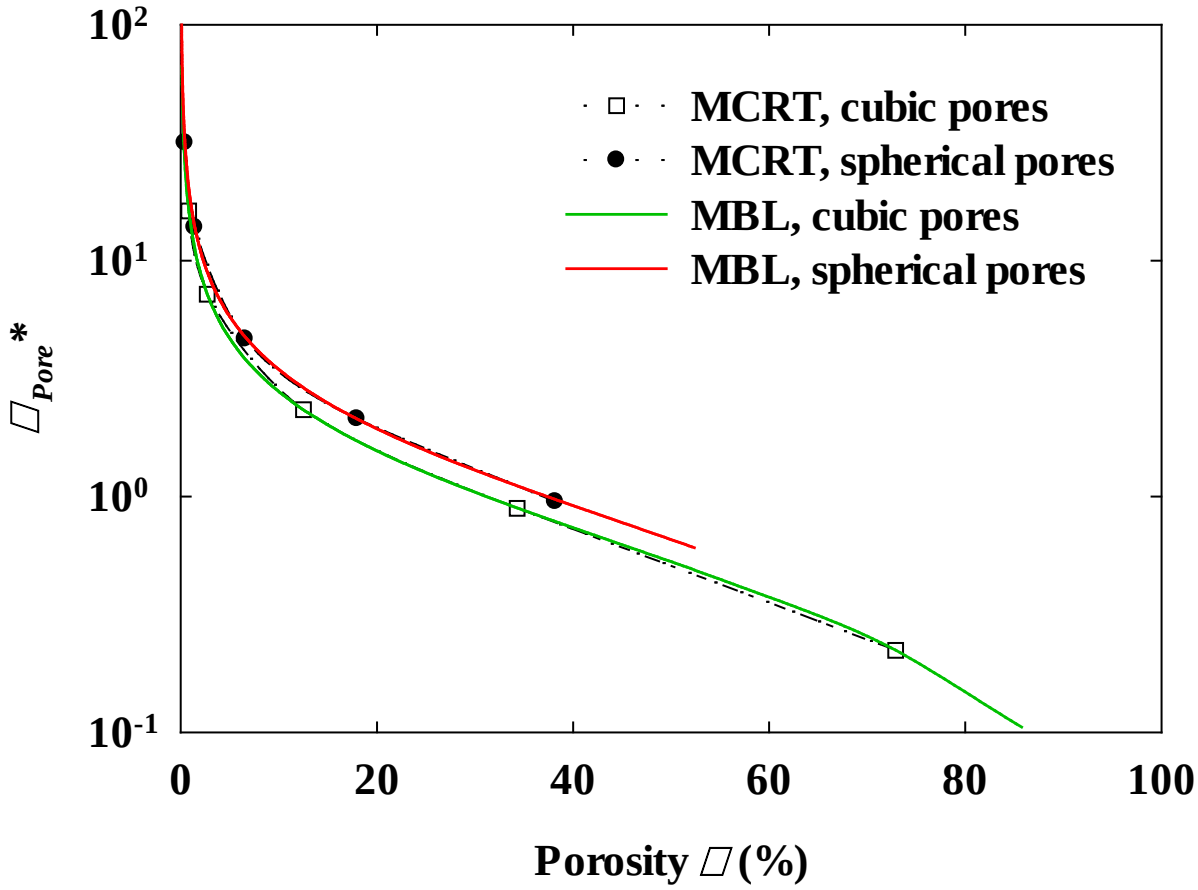
10^2
10^1
10^0
10^{-1}
τ^*_{Pore}
0
20
40
60
80
100
Porosity ϕ (%)
MCRT, cubic pores
MCRT, spherical pores
MBL, cubic pores
MBL, spherical pores

Figure 2

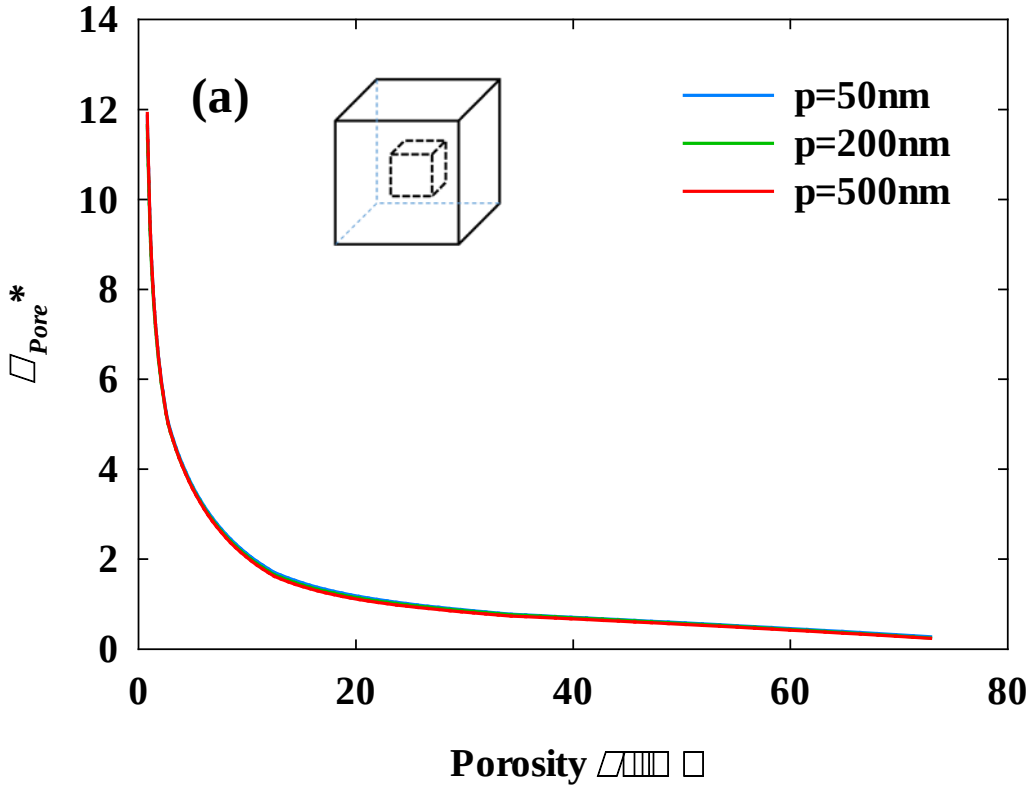
(a)
p=50nm
p=200nm
p=500nm
14
12
10
8
6
4
2
0
0
20
40
60
80
Porosity

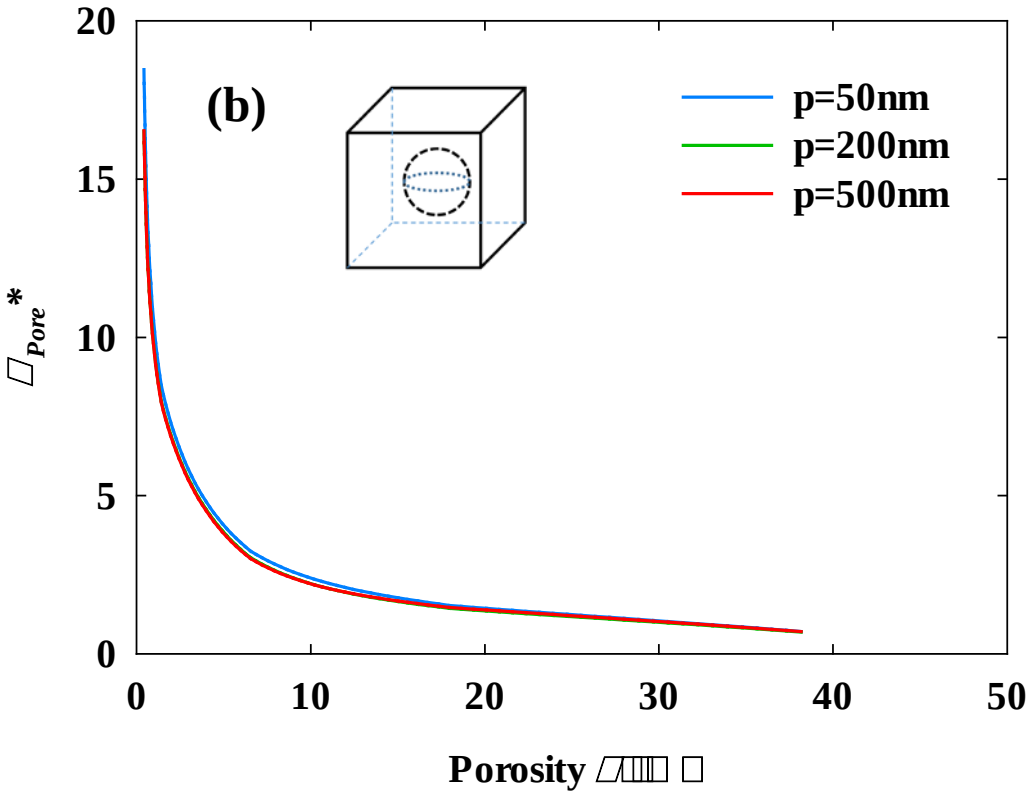
(b)
p=50nm
p=200nm
p=500nm
20
15
10
5
0
0
10
20
30
40
50
Porosity

Figure 3

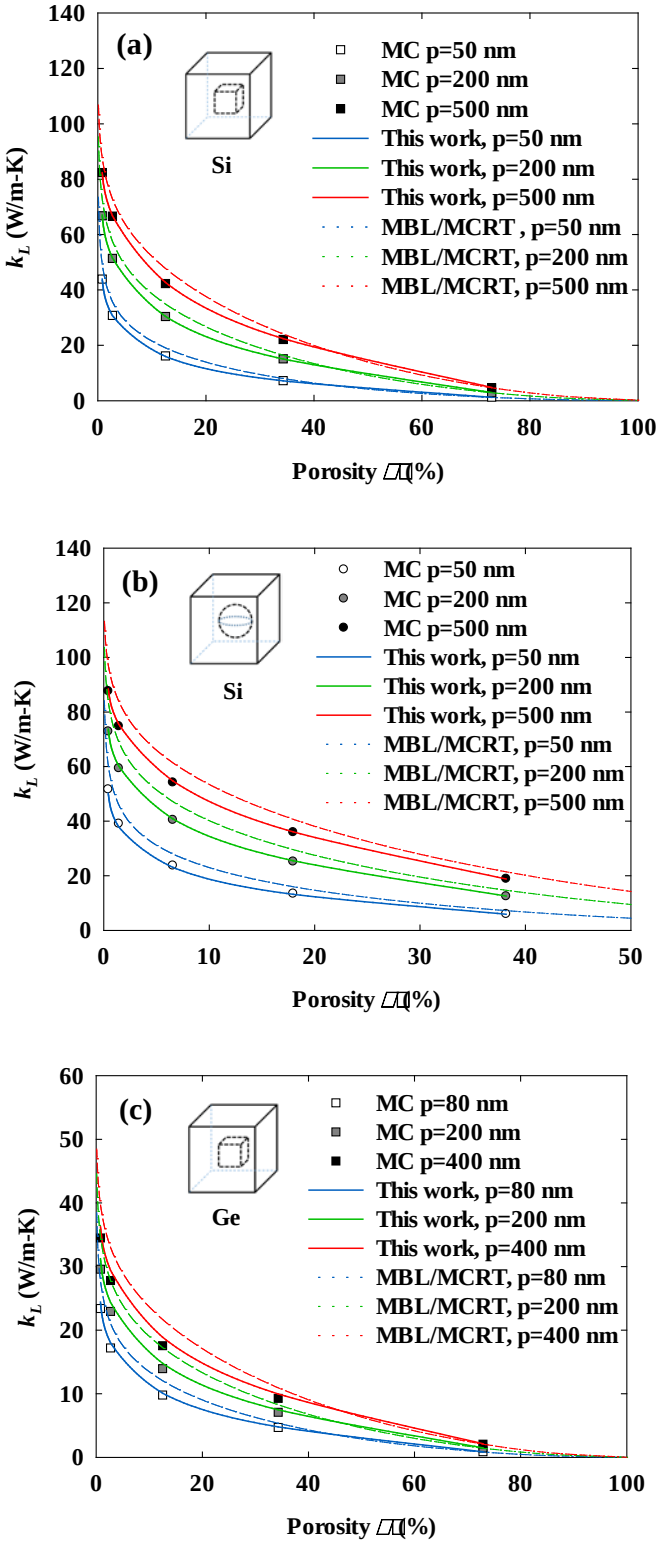
(a)
Si
MC p=50 nm
MC p=200 nm
MC p=500 nm
This work, p=50 nm
This work, p=200 nm
This work, p=500 nm
MBL/MCRT , p=50 nm
MBL/MCRT, p=200 nm
MBL/MCRT, p=500 nm
k_L (W/m-K)
Porosity (%)
(b)
Si
MC p=50 nm
MC p=200 nm
MC p=500 nm
This work, p=50 nm
This work, p=200 nm
This work, p=500 nm
MBL/MCRT, p=50 nm
MBL/MCRT, p=200 nm
MBL/MCRT, p=500 nm
k_L (W/m-K)
Porosity (%)
(c)
Ge
MC p=80 nm
MC p=200 nm
MC p=400 nm
This work, p=80 nm
This work, p=200 nm
This work, p=400 nm
MBL/MCRT, p=80 nm
MBL/MCRT, p=200 nm
MBL/MCRT, p=400 nm
k_L (W/m-K)
Porosity (%)

Figure 4

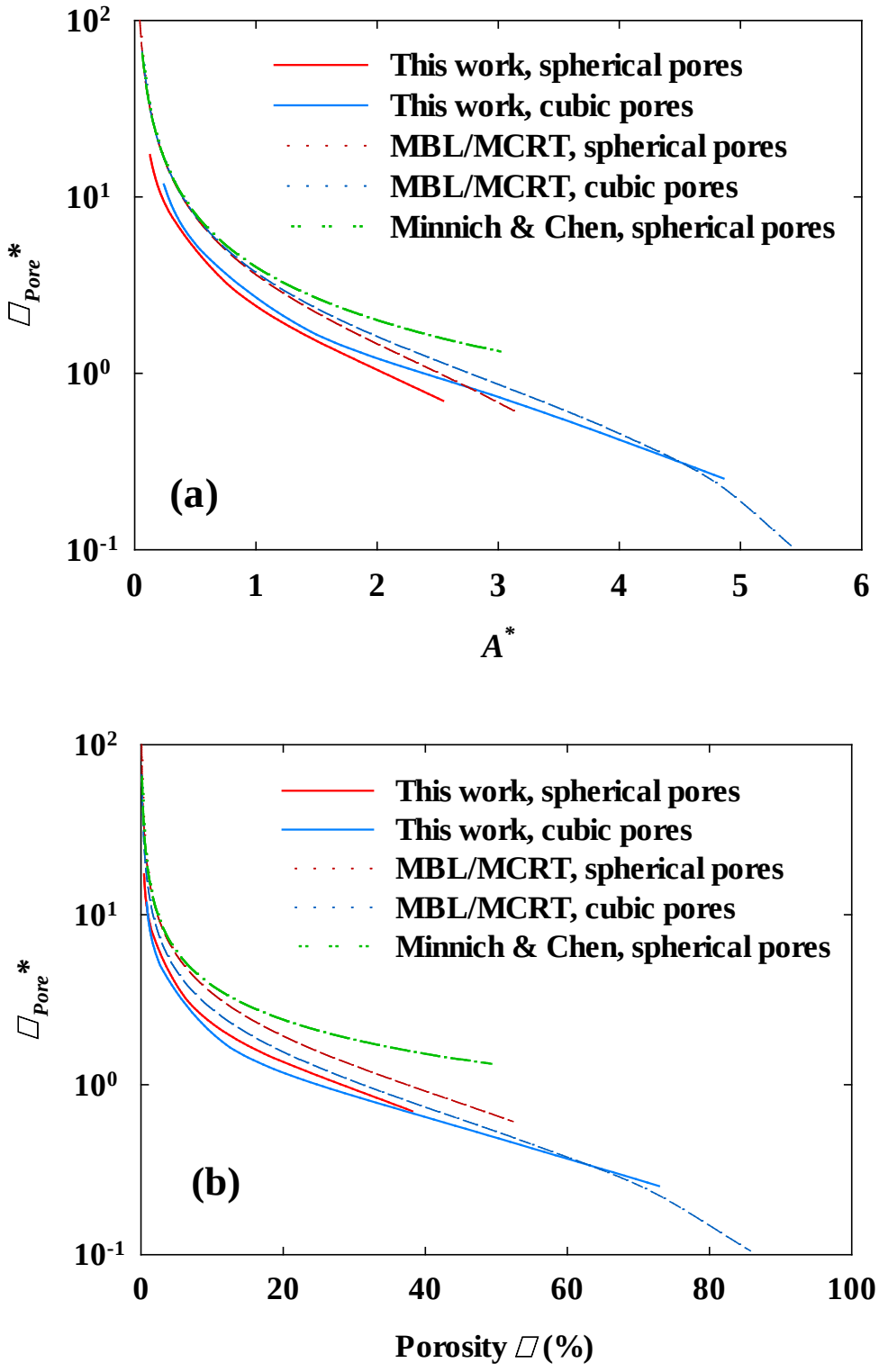
This work, spherical pores
This work, cubic pores
MBL/MCRT, spherical pores
MBL/MCRT, cubic pores
Minnich & Chen, spherical pores
(a)
(b)
τ^*_{Pore}
A^*
Porosity ε (%)

Figure 5

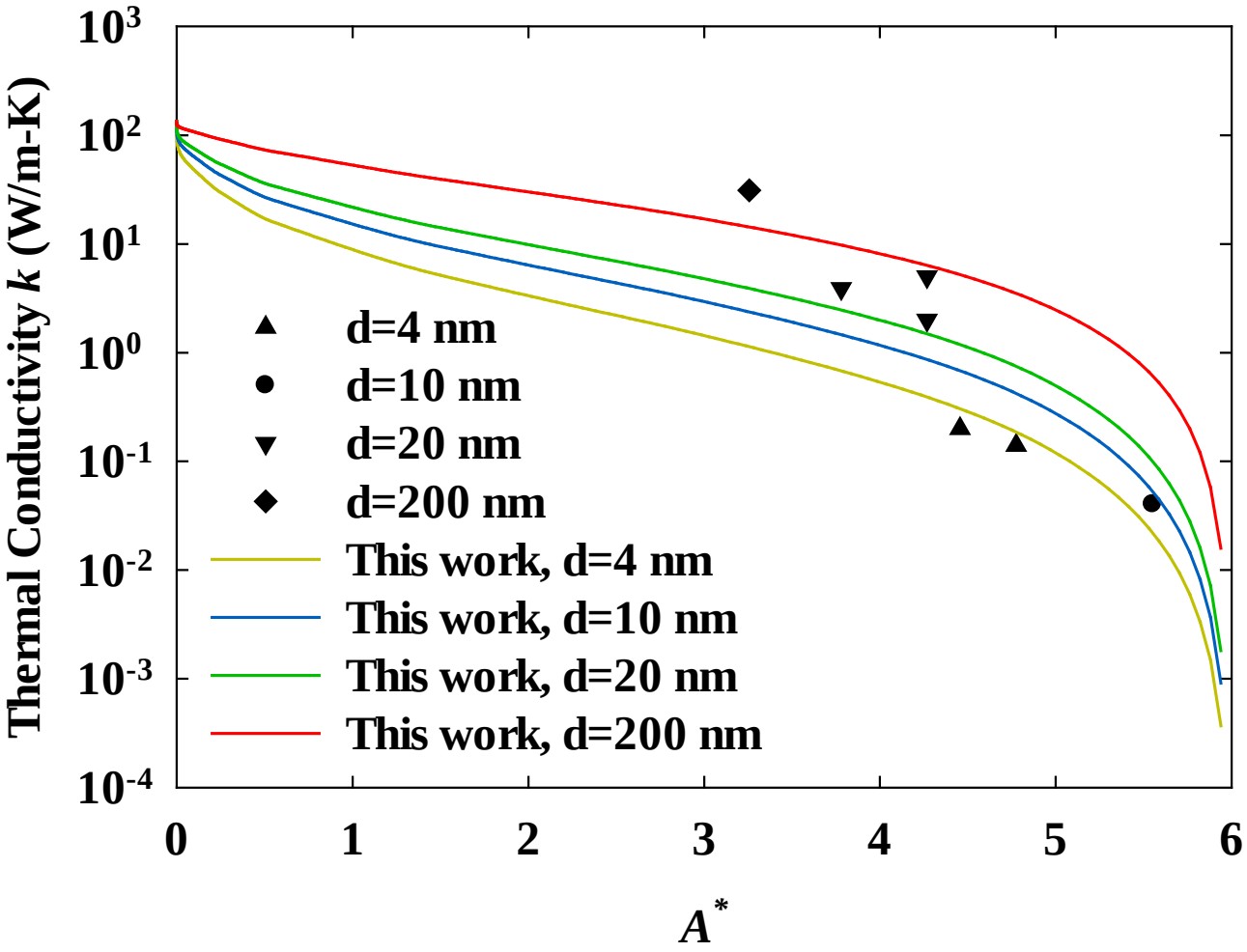
Thermal Conductivity k (W/m-K)
10^3
10^2
10^1
10^0
10^-1
10^-2
10^-3
10^-4
0
1
2
3
4
5
6
A*
d=4 nm
d=10 nm
d=20 nm
d=200 nm
This work, d=4 nm
This work, d=10 nm
This work, d=20 nm
This work, d=200 nm

Figure 6

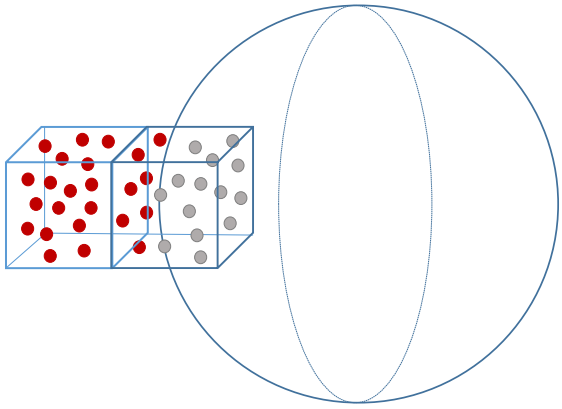

Figure A1

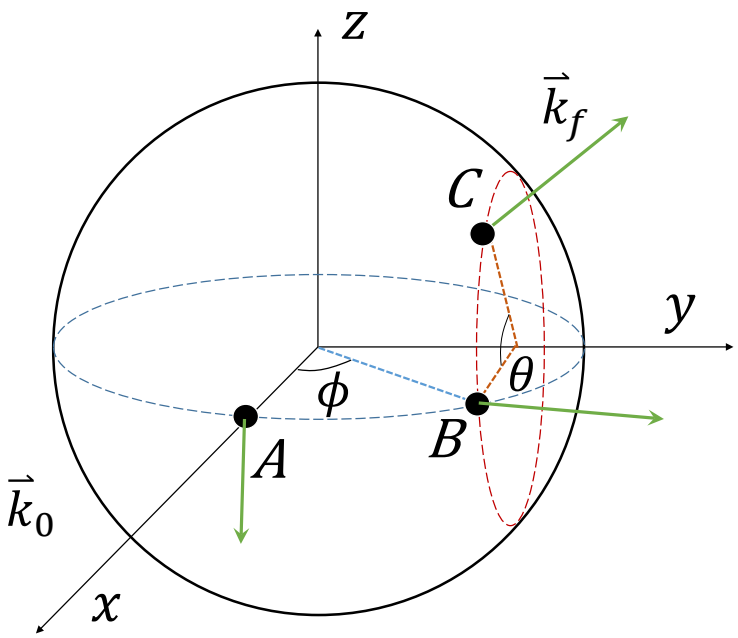

Figure A2

Table Captions

Table 1. The comparison between predicted and measured thermal conductivities of nanoporous Si.

Porosity (%)	Pore diameter (nm)	A^*	Measured k (W/m·K)	Predicted k (W/m·K)
40 [a]	200	3.26	31.2	15.2
50 [a]	20	3.78	3.9	2.5
60 [a]	20	4.27	2–5	1.51
64 [b]	4	4.46	0.2	0.31
71 [b]	4	4.77	0.14	0.17
89 [b]	10	5.55	0.04	0.05

[a] [56]. [b] [57].